Ultrafast reflectivity dynamics of highly excited Si surfaces below the melting transition

R. Gunnella,[1,2] G. Zgrablic,[3] E. Giangrisostomi,[3] F. D'Amico,[3] E. Principi,[3] C. Masciovecchio,[3]
A. Di Cicco,[1] and F. Parmigiani[3,4,5]

[1]*Sezione Fisica, Scuola di Scienze e Tecnologie, Universita di Camerino, via Madonna delle Carceri, 62032 Camerino, Italy*
[2]*CNR-ISM, via Fosso del Cavaliere, 00133 Tor Vergata, Italy*
[3]*Elettra-Sincrotrone Trieste S. C. p. A., Strada Statale 14, km 163.5, 34149 Basovizza, Italy*
[4]*Department of Physics, Universita degli Studi di Trieste, via A. Valerio 2, 34127 Trieste, Italy*
[5]*International Faculty, University of Köln, 50937 Köln, Germany*

(Received 29 October 2015; revised manuscript received 18 May 2016; published 17 October 2016)

Solid Si under intense femtosecond irradiation is investigated over a wide range of fluences below the melting transition by supercontinuum light (400–800 nm) transient reflectivity. By solving a system of time-dependent equations, the fast and slow components of the energy and carriers diffusion can be disentangled from the reflectivity data, providing considerable insight into the nonequilibrium phase-change dynamics. The study of the fluence values immediately preceding the dramatic melting transition can be useful for discriminating between the thermal and electronic origins of the disordering of the structure by looking at the modification of the solid-state properties of the Si surface.

DOI: 10.1103/PhysRevB.94.155427

I. INTRODUCTION

Initial electron excitation in solids by means of high-power femtosecond radiation after short-lived coherent polarization of the material [1] is soon followed, on time scales of around 10^{-13} s, by progressive thermalization of excited electronic states through carrier-carrier interactions [2,3]. From temperatures T_e greater than the lattice temperatures excited electrons cool down, on a time scale ranging from 10^{-13} to 10^{-12} s, by scattering of phonons [4], with the result being that severe nonequilibrium conditions in the solid need several picoseconds to fade out. In particular, before the first few hundred femtoseconds, local equilibrium temperature cannot be defined, and hybrid processes, involving event-by-event exchange between highly excited and low-energy-band state electrons, become dominant [5].

Different from metals, in which the two-temperature approach (by monitoring only the electrons and lattice temperatures) can be successful [6], in semiconductors huge changes in carrier densities can drive dramatic perturbation in the transient properties of the solids [7]. For instance, a radiation fluence of $0.2\,\mathrm{J/cm^2}$ for a photon beam impinging on a Si surface (which is able to generate up to $10^{22}\,\mathrm{cm^{-3}}$ electrons [8,9]) can induce a melting transition with a wave front traveling over 10–20 nm. At higher fluences, melting has been observed to occur in less than 1 ps by a variety of experiments using optical reflectivity [10], electron diffraction [11], time-resolved ellipsometry [12,13], and second-harmonic generation [10,14]. As any other thermal process would take one order of magnitude larger time scales, it has been concluded that femtosecond laser pulses can induce nonthermal structural changes [15,16]. This point has been the matter of contrasting speculations [5,17]: on the one hand, the change in the characteristic time scale could hint at massive electronic excitation and nonthermal processes; on the other hand, the process is claimed to be thermal even though is occurs at large fluences and fast rates.

It is nevertheless undeniable how challenging keeping track of matter evolution is under ultrashort irradiation. It is an issue that deserves great attention, especially in relation to the study of warm dense matter in the x-ray regime [5,18]. One example might be related to the observation of novel structural and electronic order-disorder phase transitions [11,19] in model covalent systems like group-IV semiconductors [20]. There, metastable state spectroscopies combined with electronic structure calculations showed that a metallic state is formed for the semiconductor crystalline silicon (c-Si) in the high-density-liquid (HDL) phase, whereas the low-density-liquid (LDL) phase is semimetallic, with a pseudogap [21–23]. The LDL phase cannot be obtained with the usual methods like decompression from a highly compressed state, ion impact [24–26], or undercooling from the equilibrium HDL phase because of the onset of an ultrafast crystallization process [27]. As a possible shortcut, ultrafast heating and release have been proposed, enabling the observation of liquid-liquid transition from an isochoric excitation to an isoentropic relaxation of the system.

Within this picture, it is important to disentangle thermal and nonthermal processes during ultrafast probing of covalent liquid-phase diagrams on both sides of the energies and the time scales of the transitions. It is also a crucial point to understand if the nonthermal processes lead to conditions of warm dense matter [18,28] or to other exotic states. In this context, we present a complete set of data to revisit, with an extended fluence and time range, the ultrafast reflectivity of Si. One unique element is the use of a supercontinuum probe to record in real time the modification of the valence states. What we obtained in this study is a clear indication that the response of the solid to the ultrafast excitation is peculiarly different when approaching the melting threshold. At the transition fluence, we observed anomalies in lattice temperatures and electron diffusion coefficients that have not been discussed in previous works.

In addition, with respect to the other evidence of the ultrafast heating of Si [29–44], our main aim is to detect possible hints of spectral and structure modification before the melting occurrence by the transient reflectivity over a large range of supercontinuum optical wavelengths. Such melting precursors possess relaxation dynamics that, in spite of the

abundant literature, still need to be properly rationalized and categorized for further studies of condensed matter in extreme nonequilibrium conditions.

II. EXPERIMENT

The experiment was performed at the T-REX laboratory in Elettra (Trieste) [45] employing a standard amplified Ti:sapphire laser working at 800 nm and frequency doubled for use as a pump (pulse width of 80 fs FWHM). The probe was obtained by focusing the laser pulses on a CaF_2 crystal to produce supercontinuum white light (SWL) in the 350–1000-nm range. The SWL was focused on the sample in spatial and temporal coincidence with the pump pulse and dispersed on a 512-pixel *n*-type metal-oxide semiconductor array, after the interaction with the sample.

Samples were commercially available Si(100) slabs (moderately B doped, *p* type, concentration below $10^{16}\,\mathrm{cm}^{-3}$). Typical spot diameters used during the experiment were 100 μm for the pump pulse and 50 μm for the probe pulse. The pulse temporal shape was accurately monitored during the experiment, and the time delay scale, which is wavelength dependent because geometry and optical elements both contribute to a spread of about 200 fs, was accurately calibrated with the ultrafast response signal of $CuGeO_3$ [45]. The superposition of the pump and probe pulses was guaranteed by a long-distance microscope (Questar CM1) with an accuracy better than 5 μm. The orientation of the crystal turned out to be not relevant [34], and the natural oxide layer acted as a passivation layer that was highly transparent to both the pump and probe radiation. The broadband change of reflectivity of the Si(100) surface was measured for different pump fluences (up to $0.03\ \mathrm{J/cm}^2$) as a function of time delay in the 0–20-ps range with different time resolutions. The experiment was performed at repetition rates of 500 and 250 Hz for the probe and pump, respectively, in order to evaluate at each delay time the corresponding change of optical density (OD):

$$-\Delta\mathrm{OD} = (\Delta R/R)/\ln(10). \quad (1)$$

The measurements were done in single-shot mode, i.e., changing the region of the surface after each pump pulse thanks to a motorized three-axis sample stage. The effects of the high-fluence pump pulses on the Si(100) surface have also been investigated using an optical microscope [42] which has shown the permanent damage of the surface for pulse fluences above the ablation threshold. Our estimation of the damage threshold for given wavelengths and duration of the pump pulse turns out to be in line with previous measurements of $F_{\mathrm{th}} = 0.03\,\mathrm{J/cm}^2$. This estimate is coincident with the observation of overshooting effects in the reflectivity [46]. At this fluence, the number of excited *e*-h pairs at the surface amounts to $N(z=0,t=0) = F_{\mathrm{th}}(1-R)/(h\nu\delta)$, where $\delta \approx 80$ nm is the penetration depth of 400-nm radiation in solid Si. The resulting estimate of about $0.3\times10^{22}\,\mathrm{cm}^{-3}$ corresponds to 6% of the atoms in solid Si, which is close to the plasma critical density [29].

III. MODELIZATION OF THE TRANSIENT REFLECTIVITY

In order to properly model the transient reflectivity, we must consider several contributions: (1) a Drude-like carrier, (2) band state filling, (3) band structure normalization, and (4) lattice temperature effects. The effects of band state filling and band structure normalization are balanced to some extent, the former resulting in an increase of the band gap due to occupation of lower excited states, the latter resulting in a shrinking at the band gap due to an increased attractive exchange potential inside the electron gas [47]. Band normalization can be expected to give an increase in the optical refractive index. Since, on the contrary, the latter is observed to decrease during the transient regime (at least in the low-fluence limit) [34], we conclude that its contribution can be neglected in the present analysis. The state-filling effect rapidly vanishes with time, and its contribution to reflectivity is negligible with respect to free carriers [37] at low fluences and long delay times ($>1--2$ ps). Finally, the well-established thermal effects on reflectivity in stationary experiments [48] will be considered to comply with the last term of lattice heating.

We start the analysis of low-fluence experiments and establish the diffusion dynamics by looking at the reflectance from the sample at different probing wavelengths. One of the main problems in studying solid-liquid transitions by ultrafast optical techniques is to disentangle the electronic and structural degrees of excitation. Hot charge carriers can diffuse at ultrasound speed and might be monitored with difficulty in a pump and probe experiment if the probe is not limited to the excitation region.

By the supercontinuum light excitation we can tune the probing depths $d_{\mathrm{probe}} = \lambda/(4\pi n)$ [37] (where n is the refractive index) from about 18 nm for 800-nm radiation up to 6 nm for a 400-nm wavelength. Such a probed volume is homogeneously excited by the pump radiation at a wavelength of 400 nm up to a depth of $\delta_{\mathrm{pump}} = \lambda/(4\pi k) \approx 80$ nm (in terms of the imaginary part k of the refractive index), as illustrated in Table I. The difference in the probed volume by varying wavelength can be exploited to obtain information about the characteristic relaxation and thermalization times. For instance, the supersound velocity of hot electrons could be singled out with respect to heat transmission at a speed in the nanometer per picosecond range.

When looking closer at the electronic transitions, excitation in Si using a photon energy less than 2.2 eV (the energy of

TABLE I. Optical parameters of Si at room and high temperature [49] at two different wavelengths λ: refractive index n, probed depth d, imaginary refractive index k, pumped depth δ, and pump reflectivity R.

	Solid Si		Liquid Si	
Parameter	400 nm	800 nm	400 nm	633 nm
n	5.6	3.6	2.3	3.8
d (nm)	5.7	17.6	6.8	12.6
k	0.383	0.005	4.7	5.2
δ (nm)	82	10^4	6.7	9.7
R	0.47	0.56	0.72	0.69

the L_1 conduction band) injects hot electrons directly into the states along the Γ-X line, which relax to the conduction-band minimum (CBM) via intravalley scattering within about 100 fs [50].

For higher photon energies that are still lower than the excitation over the direct gap (3.3 eV), an increasing absorption coefficient is related to the indirect excitation to L and/or X valleys [51], followed by intervalley scattering with large momentum transfer. In this case time-resolved two-photon photoemission showed that the relaxation time of hot electrons from the L-X valley to the CBM is increased (in the range of a few picoseconds) [52].

For this reason, by using 3.1 eV pumping radiation hot electrons will reach the conduction-band minimum in a longer time with respect to excitations with a lower-energy pump. Here, for large fluences, we expect to pinpoint surface bond rupture [53] and electronically driven order-disorder phase transitions.

The reflectivity as a function of time passes through several stages. At the first stage, coincident in time with the pump pulse, the reflectivity abruptly changes due to the formation of a dense cloud of electron-hole pairs. When 10^{22} electrons/s is exceeded (corresponding to an incident fluence of 200 mJ/cm^2), a plasma is generated [54]. Below this limit, as a result of recombination of electron-hole pairs, the reflectivity tends to recover its initial value. For relatively low intensity levels, the reflectivity returns to its initial value after a decrease in the carrier density. By contrast, at a higher level of the pump-pulse energy (in the present case larger than $0.55F_{\text{th}}$), the reflectivity is observed to increase above the initial value, as a result of disordering. Experimental transient reflectivity curves are compared to calculations according to the formula for s-polarized reflectivity at normal incidence [37], including contributions from free-carrier (FC), state-filling (SF), and lattice temperature T effects. Starting from the optical reflectivity written in terms of the refractive index n and extinction coefficient k,

$$R = \frac{(n-1)^2 + k^2}{(n+1)^2 + k^2}, \tag{2}$$

if Δn is the transient modulation of the refractive index in the approximation of the small imaginary part k, the relative change in reflectivity may be written [37] in terms of the three contributions discussed above (Δn_{FC}, Δn_{SF}, and Δn_T):

$$\begin{aligned}\Delta R/R &= \frac{4\Delta n}{n^2-1} \\ &= \frac{2[\text{erf}(t/\tau_p)+1](\Delta n_{FC} + \Delta n_{SF} + \Delta n_T)}{n(\omega)^2 - 1}.\end{aligned} \tag{3}$$

The above equation contains the temporal shape of the excitation in terms of the error function with pulse duration τ_p = 80 fs. The free-carrier contribution is modeled according to the Drude approximation describing the decrease in dielectric constant due to an increased number of carriers N_c as

$$\Delta n_{FC} = -\frac{2\pi e^2}{n_0 \omega^2} \frac{\Delta N_C}{m^*_{\text{opt}}(T_e)}, \tag{4}$$

which is easily obtained by expanding to the first order the refractive index function $n_0 = \sqrt{\epsilon_0}$ by a transient Drude contribution to the dielectric constant $\Delta\epsilon(\omega) = -(4\pi N_c e^2)/(m\omega^2)$. The optical mass $m^*_{\text{opt}} = (1/m^*_e + 1/m^*_h)^{-1}$ depends on the electronic temperature via the band nonparabolicity. Here, we parametrized it according to the data reported in Ref. [37]. Moreover, a reflectivity increase is expected in the case of a temperature increase in the solid according to Eq. (5):

$$\Delta n_T = \frac{dn}{dT}(T_A - T_{RT}), \tag{5}$$

where the temperature gradient of the refractive index is obtained from graphical interpolation of the data in Ref. [48] or, in an equivalent way, directly from the temperature gradient of reflectivity given in Ref. [49].

Here, two considerations are mandatory: (1) the use of the undamped Drude formula should be replaced close to the transition by a damped version [10,55–58]. In fact previous experiments at high fluences have measured with good accuracy a relaxation time of a few femtoseconds. For this time scale the approximation of high optical frequencies cannot be used. It is therefore straightforwardly the failure of the present model in approaching the damage threshold too closely. As estimated from Ref. [55], we must limit fluences below 25 mJ/cm^2 to no more than a 10% difference in reflectivity in the present approximation. (2) In the same approximation we neglect spatial variation of the optical properties, and consequently, we could incur the wrong estimation of the carrier density at the surface, as effectively outlined in Refs. [10,55] and also from the theoretical point of view in [56–58]. Such a refinement in the model should be used in the case of a quantitative determination of optical properties at the onset of the transition region, which is out of the scope of the present work.

To the above picture, the state-filling contribution to the transient reflectivity must be added. Such an effect is present even at the lowest fluences of the present experiment and increases with the degree of photon excitation, as can be seen in Fig. 1, which outlines the reflectivity in the first picosecond. It denotes saturation of available final states for interband transition increasingly contributing to a modified refractive index, with consequent lowering of the reflectivity, especially for wavelengths longer than the pump wavelength (400 nm). It is important to stress that this behavior is opposite to that known as reflectivity overshooting and occurring above threshold. The present case is a purely electronic effect clearly shown in Fig. 1 and is due to the large number of electronic excitations in the ultrashort time of observation.

The wavelength dependence has been modeled by a smooth step function around the middle of the spectrum, amounting to a reflectivity change of a few percent. More precisely, the state-filling contribution is calculated according to the empirical formula

$$\Delta n_{SF} = -a_{SF} \frac{N(t)}{N(0)} \frac{1}{\pi} \left[\frac{\pi}{2} - a\tan\frac{\lambda_c - \lambda}{w_\lambda}\right][(n^2(\omega) - 1)/2]. \tag{6}$$

Here, λ_c is the state-filling centroid wavelength, and a_{SF} is a factor ranging from 0.1 to 1.0 from lower to higher fluences. The above equation has been checked for a more rigorous approach based on the dispersion relations [59] of the transient absorption. According to the following equation, as suggested by Sabbah and Riffe [37], the exponential tails effects in the

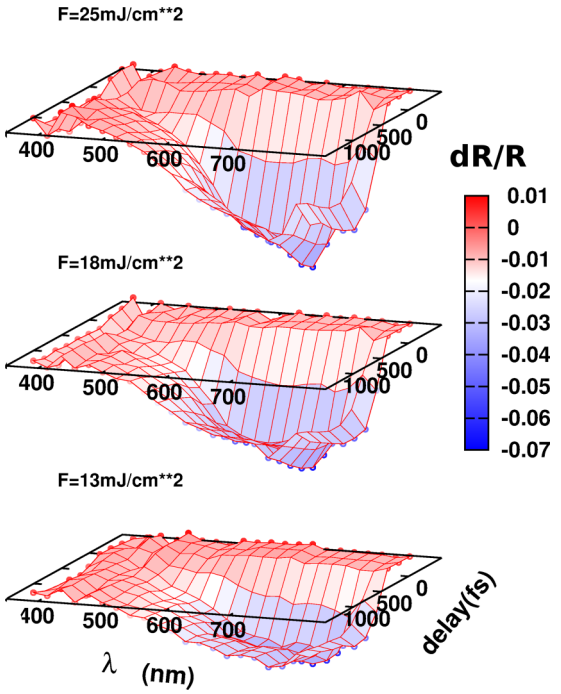

FIG. 1. First stages of reflectivity changes, showing the buildup of state filling, consisting of a wavelength dependence that grows with increasing photon fluence, from 13 (bottom) to 25 mJ/cm^2 (top).

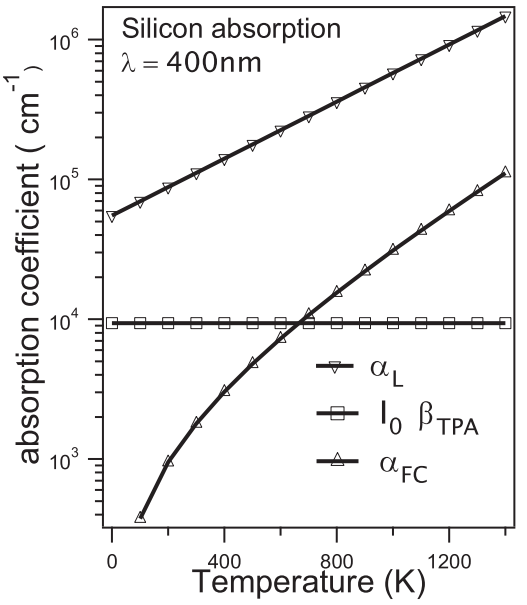

FIG. 2. Numerical estimation of one-photon (α_L) and two-photon ($I_0\beta_{TPA}$) absorption in Si. Also reported is the free-carrier absorption contribution α_{FC}.

absorption at the band edges contribute by

$$n(\lambda) = 1 + \lambda \int \frac{d\lambda'}{4\pi} \frac{\alpha(\lambda')}{(\lambda^2 - \lambda'^2)}. \tag{7}$$

Although a computationally demanding approach is needed close to threshold when event-by-event interaction of high-energy electrons with the low-energy solid band electrons [5] is dominant, well below such a limit (25 mJ/cm^2) we can make use of a simplified rate equation for the population of photocarriers.

By the following diffusion rate equation, the variation in the number of carriers is expressed in terms of characteristic constants like the diffusion coefficient $D(N_C)$, Auger generation parameter γ, and single- (α) and double-photon (β_{TPA}) absorption:

$$\frac{\partial N_C}{\partial t} = \frac{\partial}{\partial z}\left[D(N_C)\frac{\partial N_C}{\partial z}\right] - \gamma N_C^3 + \frac{(1-R)}{E_{\rm ph}}\left(I\alpha + \frac{1}{2}\beta_{TPA} I^2\right). \tag{8}$$

The two-photon/single-photon absorption ratio is $\beta_{TPA}F(1-R)/(2\alpha\tau_p)$ in terms of fluence, reflectivity, and temporal pulse width. At $\lambda = 400$ nm and $\tau_p = 80$ fs characteristic values are $\alpha = 10^5\,\mathrm{cm}^{-1}$ and $\beta = 65\,\mathrm{cm}\,GW^{-1}$. Therefore, we expect that before melting the ratio amounts to less than 10%, as can be observed in Fig. 2.

Consistent solutions for ΔN, phonon temperatures T_O, T_A, and carrier temperature T_C are given numerically over a 700 × 700 grid with a nonconstant mesh and initial steps of 5 nm along z and of 0.4 fs in time. The Crank-Nicolson method [60] is used so that we have an unconditionally stable solution. The step size Δt has been chosen on the basis of truncation error, independent of the Δz variation. With respect to the GaAs or InSb cases, considered in the work by Rämer *et al.* [7], silicon has the advantage that the difference between electron and hole masses is less than 20% and the two carriers can be expressed by a single equation.

The recombination of the e-h pairs will follow mainly the Auger mechanism, especially at the very early stages, as described by the second term on the right-hand side of Eq. (8) with a multiplicative constant γ of around $6 \times 10^{-31}\,\mathrm{cm}^6\,\mathrm{s}^{-1}$ [31]. The Auger decay will depend on the electron and hole densities, which release their annihilation energy by reheating already out-of-equilibrium electrons (hence the N^3 dependence). Due to the strong recombination at the defects present on the surface (the interface with the native oxide), an additional recombination term following Ref. [61] is used to set the Neumann boundary conditions of Eq. (8). Its value is close to 1.5×10^4 cm/s.

The diffusion coefficient $D(N_C)$, about $18 \times 10^{-4}\,\mathrm{cm}^2/\mathrm{s}$ at room temperature in the dark, depends on the number of photocarriers. A possible description, following Li and coworkers [62], indicates that around an excited electron density of $10^{19}\,\mathrm{cm}^{-3}$, the diffusion coefficient is reduced by carrier-carrier scattering. The last effect is mitigated at higher densities ($\geqslant 10^{19}\,\mathrm{cm}^{-3}$) by a strong screening effect. In these conditions, comparable to the experiment reported here, an increase of 40% or more in diffusivity is observed as a consequence of a 10% screening of the electron charge. For the above reasons we allowed this parameter to vary during the best-fit procedure.

In addition to Eq. (8), the energy transfer between the various relaxation channels in the solid [63] is described

by

$$\frac{\partial E_C}{\partial t} = \frac{\partial}{\partial z}\left[\left(E_g + \frac{2}{3}\frac{E_C}{N_C}\right)D_{NC}\frac{\partial N_C}{\partial z}\right] + \gamma\left(E_g + \frac{1}{2}\frac{E_c}{N_c}\right)N_C^3 + \frac{\partial}{\partial z}\left(K_{Tc}\frac{\partial}{\partial z}T_c\right) - \frac{(E_{\rm ph} - E_g)}{E_{\rm ph}}I\alpha - \frac{(E_C - C_C T_O)}{\tau_{CO}} - \frac{(E_C - C_C T_A)}{\tau_{CA}}. \quad (9)$$

Here, the first term in the local energy density change is represented by the kinetic energy diffusion of hot electrons and holes; the second term is the boosting of carriers from the recombination of high-energy Auger processes where potential energy is imparted to existing nonequilibrium carriers; the third term is the thermal conduction of hot electrons with quasiequilibrium temperature T_C. Phenomenological relaxation of electron energy into the conduction band and into the vibrational degrees of freedom is described by Eq. (10). There, the optical phonon thermal population T_O and the acoustic phonon temperature T_A are related by phenomenological relaxation-time constants of carrier energy to optical phonon excitations τ_{CO}, carrier energy to acoustic phonon vibrations τ_{CA}, and optical phonon to acoustic phonon conversion τ_{OA}.

Characteristic values are $\approx$0.2 ps for the energy transfer from hot carriers to optical phonons [64] and larger than 1 ps for the transfer from hot carriers to acoustic phonons [32]. Finally, several tens of picoseconds are needed for the energy transfer from optical to acoustic phonons [64]. This scheme well reflects the mesoscopic effect [65] in semiconductors. In fact, at high temperatures, electron energy is better transferred to optical phonons than to lattice vibrations directly. For this reason we find it useful to introduce two different channels of relaxation of the carrier excess energy.

It is important to keep in mind that the increase in reflectivity with the temperature is due to redshift of the exciton energy. The exciton-phonon coupling is responsible for the Stokes energy shift in the transition at the band edge and the consequent significant reflectivity increase. We can claim with reasonable confidence that optical properties are modified by anharmonic effects due to thermal expansion. Such an expansion is more likely to occur when enough energy is stored in the low-energy transverse acoustic phonons [66], and for this reason such an increase is less effective in the first 1–2 ps, where the role is mainly played by the optical phonons.

Optical phonon and acoustic phonon temperatures can be obtained from the following set of rate equations:

$$\frac{\partial T_O}{\partial t} = C_C(N_C)\frac{(T_C - T_O)}{\tau_{CO}C_O} - \frac{(T_O - T_A)}{\tau_{CA}},$$
$$\frac{\partial T_A}{\partial t} = \frac{\partial}{\partial z}\left[D_T(T_A)\frac{\partial T_A}{\partial z}\right] + C_O(T_O)\frac{(T_O - T_A)}{(\tau_{OA}C_A)} + C_C(N_C)\frac{(T_C - T_A)}{\tau_{CA}C_A}. \quad (10)$$

Here, the transient carrier-specific heat is obtained from $C_C(N_C) = 2 \times 3/2 k_B N_C$, where the factor 2 accounts for electrons and holes. Following van Driel [31], the carrier-specific heat is increased by 25% as a result of the exact Fermi-Dirac integral factor $\frac{\mathcal{F}_{3/2}(\eta)}{\mathcal{F}_{1/2}(\eta)}$. In terms of Einstein ($\theta_E$)

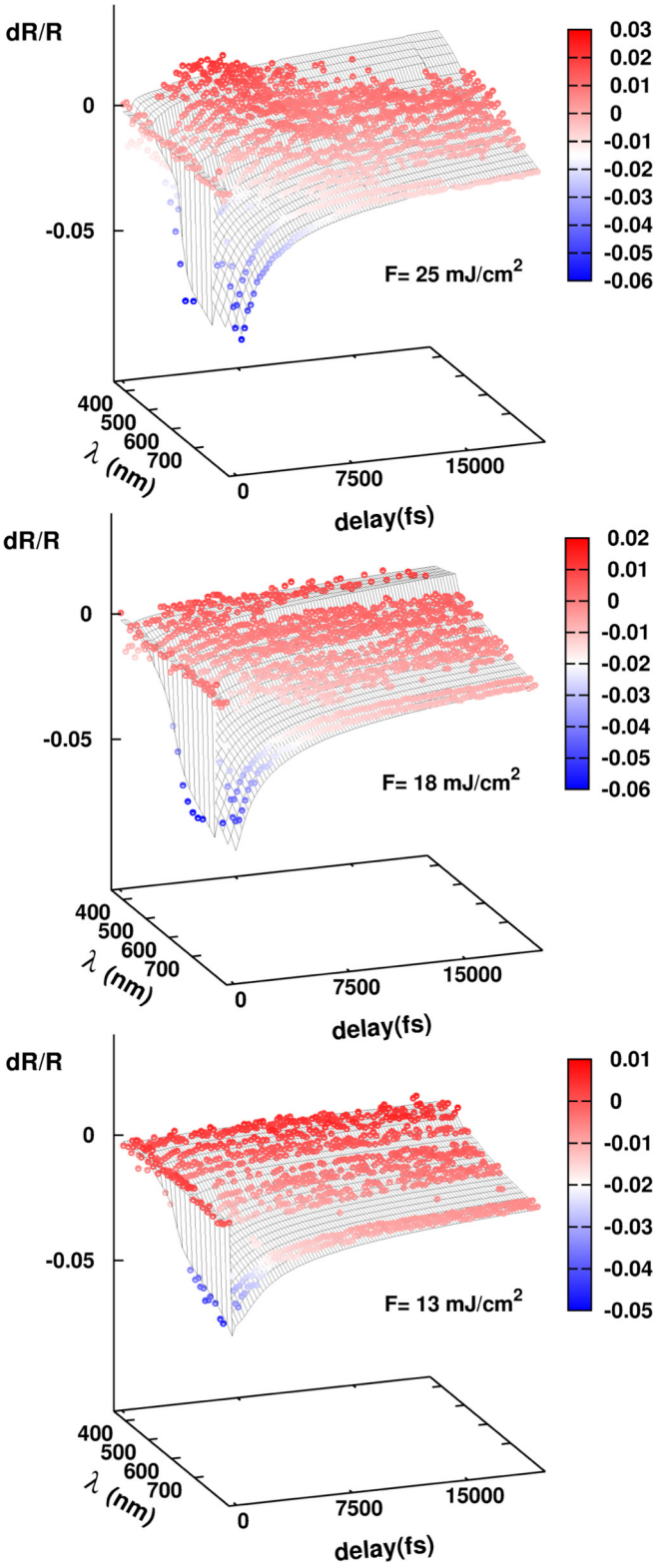

FIG. 3. From bottom to the top the complete visualization of three selected experiments at 13, 18, and 25 mJ/cm^2 fluences are reported, respectively. The color scale reports the experimental transient reflectivity change, while the gray pattern represents the modelization obtained with the diffusion rate equations.

and Debye (θ_D) temperatures the optical phonon heat capacity can be written as

$$C_O(T_O) = 2.066 \times 10^{-5} \frac{(\theta_E/T_O)^2 e^{\theta_E/T_O}}{(e^{\theta_E/T_O} - 1)^2}, \quad (11)$$

while for the acoustic phonons the formula reported by Kittel [66] can be used:

$$C_A(T_A) = 2.066 \times 10^{-5} - 9.91 \times 10^{-7} (\theta_D/T_A)^{1.948}. \quad (12)$$

Both Eqs. (11) and (12) are expressed in erg $\mu m^{-3} m K^{-1}$. The carrier thermal conductivity appearing in Eq. (9) is taken equal to

$$K_{T_C} = K_B^2 (T_C/q) N_c \mu_C^0 \frac{\mathcal{F}_0(\eta_c)}{\mathcal{F}_{1/2}(\eta_c)} \times \left[6\mathcal{F}_2(\eta_c)\mathcal{F}_0(\eta_c) - \frac{4\mathcal{F}_1(\eta_c)^2}{\mathcal{F}_0(\eta_c)^2} \right], \quad (13)$$

where μ_C^0 is the electron mobility in Si (1000 $cm^2\ V^{-1}\ s^{-1}$) and the reduced Fermi levels η_c are taken at the midgap [31]. In this work, the free-electron approximation will be used, where the parabolic effective masse are parametrized from Ref. [37].

IV. RESULTS AND DISCUSSION

In this section we report the detailed analysis of experiments done at fluences lower than the damage threshold [42]. In Fig. 3 we show three selected comparisons between experimental and calculated transient reflectivity from 13 to 25 mJ/cm^2 fluences. Parameters that are allowed to vary within a best-fit procedure are reported in Table II. They are the state-filling factor, the surface recombination velocity, the diffusion coefficient, and the three characteristic time constants. The indetermination of the parameters has been evaluated on the basis of a 20% variation of the best χ^2 value corresponding to a relative error smaller than 10%.

From the plots of Fig. 3 the level of agreement of theory and experiment is homogeneous, and all parameters are consistent across the whole set of data below the damage threshold. The number of parameters is statistically consistent with the size of the data set, according to χ^2 values.

Approaching the threshold fluence, the agreement between theory and experiment is lower (see top panel of Fig. 3), with an overall increase in reflectivity except for the high-photon-energy side of the spectrum, where the increase in reflectivity is overestimated by the model. The region of the spectrum where the reflectivity increases with respect to the theoretical expectation indicates the occurrence of metalization and the onset of a strongly disordered phase. On the other side the reflectivity in the short-wavelength range is overestimated by the theory. This indicates that at the level of excitation just preceding the threshold a relevant number of electrons are present, giving rise to a plasmonic cutoff frequency of the reflectivity. Such a cut in wavelength can be estimated from the measurements to be around 400 nm after 5 ps and 500 nm after 10 ps, corresponding, respectively, to 6.9×10^{21} and $4.9 \times 10^{21}\ cm^{-3}$ density of electrons, in full agreement with the initial excitation estimated to be around 6% of all Si atoms. This is a clear hint that the intrinsic behavior of the solid was modified by the powerful excitation and is predominantly of electronic origin rather than thermal.

A substantial reformulation within a more complex model would be necessary in order to follow the experiment above the damage threshold and will be the object of a future work. In Fig. 4 we report the temporal behavior of excited electrons,

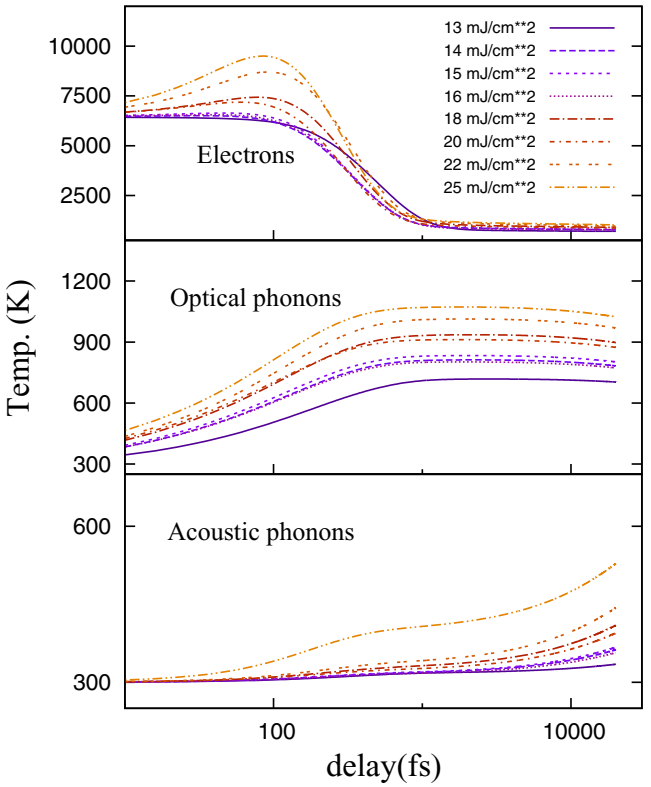

FIG. 4. From bottom to top, the temperature values of the lattice, optical phonons, and hot electrons resulting from the application of the model (as discussed in the main text) are reported at various fluences from 13 to 25 mJ/cm^2. The temperatures are obtained after an average over the probed volume extending 5–20 nm from the surface, corresponding to a volume homogeneously heated by the pump pulse (absorbed within a depth of 80 nm).

TABLE II. Resulting fitting parameters as a function of fluence: the state-filling coefficient, the surface recombination velocity (SRV), the diffusion coefficient, and the three characteristic relaxation times, τ_{CO}, τ_{CA}, and τ_{OA}.

Fluence (mJ/cm^2)	a_{SF} (%)	SRV	D_{N_c} ($\times 10^{-4}\ cm^2/s$)	τ_{CO} (ps)	τ_{CA} (ps)	τ_{OA} (ps)
13	5(1)	0.1(1)	50(10)	0.3(1)	4.0(5)	> 100
16	10(1)	0.5(1)	50(10)	0.2(1)	4.0(5)	> 100
22	10(1)	1.3(1)	36(10)	0.17(5)	3.3(5)	> 100
25	18(2)	2.0(1)	20(10)	0.15(5)	1.2(5)	> 100

optical phonons, and lattice temperatures averaged over the probed sample volume (see Table II).

From the fit parameters reported in Table II, it emerges that, at early temporal stages, thermal diffusion in the lattice is not activated yet. Melting in the solid is not accompanied by a corresponding increase in acoustic phonon temperature (T_A is found to be lower than 600 K), as evaluated by the variation of surface reflectivity on the basis of high-temperature experiments [49]. Taking into account the short time scales involved (about 0.2 ps), this observation points to an ultrafast disordering driven by nonequilibrium electrons through the high-frequency optical phonons. At the increase of the excitation fluence, the relaxation time of energy transfer from electrons to phonons decreases from 0.3 to 0.2 ps. A similar increase in rate is seen also for the carrier to acoustic phonon energy transfer, whose characteristic time is changed from 4 to 1.2 ps close to the threshold.

A larger electron diffusion coefficient (by about a factor of 2–3) is observed for fluences above 13 $\mathrm{mJ/cm^2}$, with respect to the case of room-temperature diffusion in Si. Such behavior is significantly different from the case of electron diffusion in liquid Si, about 20 times slower than in solid Si. This could indicate that coupling between electrons and phonons is at the basis of the fast melting but mostly of nonthermal character.

We should also consider the expected closure of the gap at the solid-liquid transition, i.e., the onset of metallic properties. As far as evidenced by our data set, such a transition is probably not occurring in the first 1–2-ps scale, as the state-filling effect is even stronger at the threshold fluence, while it would be heavily reduced in the case of a gap closure. The non-negligible contribution of state filling is further evidence that an electronic process is dominating the transition.

Looking at the temperature evolutions in Fig. 4, it can be clearly seen that such a transition is completed after 22 $\mathrm{mJ/cm^2}$, pointing to a strong modification of the atomic potential induced by the pump laser occurring in the first picosecond.

The emerging picture is largely in contrast to the usual thermal melting process when atomic vibrations are increasingly large and isotropic before the transition.

Here, the transition is towards a state different from the conventional liquid state. Such a transition during intense irradiation could start from an instability in the transverse acoustic (TA) Γ-point phonons with shear deformation [67] due to massive occupation of the electronic antibonding states of the conduction-band bottom [15]. For symmetry reasons, the role of longitudinal optical (LO) phonons was already invoked by Jackse and Pasturel [23] at the origin of the coupling with transverse acoustic (TA) phonons to trigger an anharmonic interaction of hot electrons with high-energy phonons, long before the transition takes place, when it is no longer possible to describe the vibrational system by the phonon approximation. In fact, in the case of Si, with respect to GaAs, this mechanism is complicated by the reduced occupation of antibonding sites because of the indirect gap and the high value of the direct gap (3.3 eV), which cannot be probed by pumped photoelectrons.

V. CONCLUSIONS

Ultrafast excitation of carriers in Si was described by a supercontinuum spectrum allowing us to single out the precursor signatures of nonthermal melting transitions in the solid. The picture outlined corresponds only in part to an order-disorder phase transition but shed light on a dynamical modification of semiconductor electronic states occurring just before the transition to a liquid with metallic overshooting reflectivity. The signatures of this modification are the widening of the Si gap, the reduction of the carrier diffusion, and the anharmonic phonon interaction long before the transition takes place.

ACKNOWLEDGMENTS

We thank the T-REX laboratory for hosting the present experiments. We acknowledge the TIMEX collaboration financed by the ELETTRA synchrotron radiation facility in Trieste and the University of Camerino. R.G. and A.D.C thank the COST Action MP1306 EUSpec.

[1] P. C. Becker, H. L. Fragnito, C. H. Brito Cruz, R. L. Fork, J. E. Cunningham, J. E. Henry, and C. V. Shank, Phys. Rev. Lett. **61**, 1647 (1988).
[2] A. Kaiser, B. Rethfeld, M. Vicanek, and G. Simon, Phys. Rev. B **61**, 11437 (2000).
[3] B. Rethfeld, A. Kaiser, M. Vicanek, and G. Simon, Phys. Rev. B **65**, 214303 (2002).
[4] J. R. Goldman and J. A. Prybyla, Phys. Rev. Lett. **72**, 1364 (1994).
[5] N. Medvedev, H. O. Jeschke, and B. Ziaja, New J. Phys. **15**, 015016 (2013).
[6] B. Y. Mueller and B. Rethfeld, Phys. Rev. B **87**, 035139 (2013).
[7] A. Rämer, O. Osmani, and B. Rethfeld, J. Appl. Phys. **116**, 053508 (2014).
[8] P. Stampfli and K. H. Bennemann, Phys. Rev. B **42**, 7163 (1990).
[9] D. von der Linde, K. Sokolowski-Tinten, and J. Bialkowski, Appl. Surf. Sci. **109–110**, 1 (1997).
[10] D. Hulin, M. Combescot, J. Bok, A. Migus, J. Y. Vinet, and A. Antonetti, Phys. Rev. Lett. **52**, 1998 (1984).
[11] M. Harb, R. Ernstorfer, C. T. Hebeisen, G. Sciaini, W. Peng, T. Dartigalongue, M. A. Eriksson, M. G. Lagally, S. G. Kruglik, and R. J. Dwayne Miller, Phys. Rev. Lett. **100**, 155504 (2008).
[12] A. M.-T. Kim, J. P. Callan, C. A. D. Roeser, and E. Mazur, Phys. Rev. B **66**, 245203 (2002).
[13] L. Huang, J. P. Callan, E. N. Glezer, and E. Mazur, Phys. Rev. Lett. **80**, 185 (1998).
[14] P. Saeta, J.-K. Wang, Y. Siegal, N. Bloembergen, and E. Mazur, Phys. Rev. Lett. **67**, 1023 (1991).
[15] C. V. Shank, R. Yen, and C. Hirlimann, Phys. Rev. Lett. **50**, 454 (1983).

[16] P. L. Silvestrelli, A. Alavi, M. Parrinello, and D. Frenkel, Phys. Rev. Lett. **77**, 3149 (1996).
[17] E. G. Gamaly, Phys. Rep. **508**, 91 (2011).
[18] B. Nagler, U. Zastrau, R. R. Fustli, S. M. Vinko, T. Whitcher, A. J. Nelson, R. Sobierajski, J. Krzywinski, J. Chalupsky, E. Abreu *et al.*, Nat. Phys. **5**, 693 (2009).
[19] M. Hase, M. Kitajima, A. Constantinescu, and H. Petek, Nature (London) **426**, 51 (2003).
[20] M. Beye, F. Sorgenfrei, W. F. Schlotter, W. Wurth, and A. Foehlisch, Proc. Natl. Acad. Sci. USA **107**, 16772 (2010).
[21] P. Ganesh and R. E. Cohen, J. Phys. Condens. Matter **21**, 064225 (2009).
[22] S. S. Ashwin, U. V. Waghmare, and S. Sastry, Phys. Rev. Lett. **92**, 175701 (2004).
[23] N. Jakse and A. Pasturel, Phys. Rev. Lett. **99**, 205702 (2007).
[24] S. K. Deb, M. Wilding, M. Somayazulu, and P. F. McMillan, Nature (London) **414**, 528 (2001).
[25] A. Hedler, S. L. Klaumunzer, and W. Wesch, Nat. Mater. **3**, 804 (2004).
[26] P. F. McMillan, Nat. Mater. **3**, 755 (2004).
[27] S. Ansell, S. Krishnan, J. J. Felten, and D. L. Price, J. Phys. Condens. Matter **10**, L73 (1998).
[28] N. Medvedev, U. Zastrau, E. Förster, D. O. Gericke, and B. Rethfeld, Phys. Rev. Lett. **107**, 165003 (2011).
[29] E. J. Yoffa, Phys. Rev. B **21**, 2415 (1980).
[30] A. Leitola and J. F. Gibbons, J. Appl. Phys. **53**, 3207 (1982).
[31] H. M. van Driel, Appl. Phys. Lett. **44**, 617 (1984).
[32] D. Agassi, J. Appl. Phys. **55**, 4376 (1984).
[33] M. C. Downer and C. V. Shank, Phys. Rev. Lett. **56**, 761 (1986).
[34] K. Sokolowski-Tinten, J. Bialkowski, and D. von der Linde, Phys. Rev. B **51**, 14186 (1995).
[35] T. Tanaka, A. Harata, and T. Sawada, J. Appl. Phys. **82**, 4033 (1997).
[36] J. Linros, J. Appl. Phys. **84**, 275 (1998).
[37] A. J. Sabbah and D. M. Riffe, Phys. Rev. B **66**, 165217 (2002).
[38] S. I. Ashitkov, M. B. Agranat, P. S. Kondratenko, S. I. Anisimov, V. E. Fortov, V. V. Tenmov, K. Sokolowski-Tinten, B. Rethfeld, P. Zhou, and D. van der Linde, JETP Lett. **76**, 461 (2002).
[39] S. I. Ashitkov, A. V. Ovchinnikov, and M. B. Agranat, JETP Lett. **79**, 529 (2004).
[40] S. H. Lee, J. Mech. Sci. Tech. **19**, 1378 (2005).
[41] D. P. Korfiatis, K.-A. T. Thoma, and J. C. Vardaxoglou, J. Phys. D **40**, 6803 (2007).
[42] A. Di Cicco, F. D'Amico, G. Zgrablic, E. Principi, R. Gunnella, F. Bencivenga, C. Svetina, C. Masciovecchio, F. Parmigiani, and A. Filipponi, J. Non-Cryst. Solids **357**, 2641 (2011).
[43] R. Gunnella, M. Ali, M. Abbas, F. D'Amico, E. Principi, and A. Di Cicco, Phys. Rev. Lett. **107**, 166103 (2011).
[44] N. Medvedev, Z. Li, and B. Ziaja, Phys. Rev. B **91**, 054113 (2015).
[45] C. Giannetti, G. Zgrablic, C. Consani, A. Crepaldi, D. Nardi, G. Ferrini, G. Dhalenne, A. Revcolevschi, and F. Parmigiani, Phys. Rev. B **80**, 235129 (2009).
[46] B. Ziaja, N. Medvedev, V. Tkachenko, T. Maltezopoulos, and W. Wurth, Sci. Rep. **5**, 18068 (2015).
[47] A. Walsh, J. L. F. Da Silva, and S.-H. Wei, Phys. Rev. B **78**, 075211 (2008).
[48] G. E. Jellison, Jr. and H. H. Burke, J. Appl. Phys. **60**, 841 (1986).
[49] G. E. Jellison, Jr. and F. A. Modine, J. Appl. Phys. **76**, 3758 (1994).
[50] T. Ichibayashi and K. Tanimura, Phys. Rev. Lett. **102**, 087403 (2009).
[51] D. E. Aspnes and A. A. Studna, Phys. Rev. B **27**, 985 (1983).
[52] T. Ichibayashi, S. Tanaka, J. Kanasaki, K. Tanimura, and T. Fauster, Phys. Rev. B **84**, 235210 (2011).
[53] J. Kanasaki and K. Tanimura, Phys. Rev. B **66**, 125320 (2002).
[54] P. Balling and J. Schou, Rep. Prog. Phys. **76**, 036502 (2013).
[55] K. Sokolowski-Tinten and D. von der Linde, Phys. Rev. B **61**, 2643 (2000).
[56] M. Combescot and R. Combescot, Phys. Rev. B **35**, 7986 (1987).
[57] B. E. Sernelius, Phys. Rev. B **40**, 12438 (1989).
[58] B. E. Sernelius, Phys. Rev. B **43**, 7136 (1991).
[59] F. Stern, Phys. Rev. **133**, A1653 (1964).
[60] H. Press, S. A. Teukolsky, W. T. Vetterling, and P. B. Flannery, *Numerical Recipes*, 3rd ed. (Cambridge University Press, Cambridge, 2007).
[61] A. Sabbah and D. Riffe, J. Appl. Phys. **88**, 6954 (2000).
[62] C.-M. Li, T. Sjodin, and H.-L. Dai, Phys. Rev. B **56**, 15252 (1997).
[63] F. S. Krasniqi, S. L. Johnson, P. Beaud, M. Kaiser, D. Grolimund, and G. Ingold, Phys. Rev. B **78**, 174302 (2008).
[64] A. Raman, D. G. Walker, and T. S. Fisher, Solid State Electron. **47**, 1265 (2003).
[65] A. A. Grinberg and S. Luryi, Phys. Rev. Lett. **65**, 1251 (1990).
[66] C. Kittel, *Introduction to Solid State Physics*, 6th ed (Wiley, New York, 1986).
[67] P. Stampfli and K. H. Bennemann, Phys. Rev. B **49**, 7299 (1994).